Applied Energy 97 (2012) 569–576

Contents lists available at SciVerse ScienceDirect

Applied Energy

journal homepage: www.elsevier.com/locate/apenergy

Steam injection experiments in a microturbine – A thermodynamic performance analysis

Ward De Paepe [a,*], Frank Delattin [a], Svend Bram [a,b], Jacques De Ruyck [a]

[a] Vrije Universiteit Brussel, Dept. of Mechanical Engineering (MECH), Pleinlaan 2, 1050 Brussel, Belgium
[b] Erasmushogeschool Brussel, Dept. of Industrial Sciences and Technology, Nijverheidskaai 170, 1070 Brussel, Belgium

ARTICLE INFO

Article history:
Received 18 July 2011
Received in revised form 31 December 2011
Accepted 20 January 2012
Available online 16 February 2012

Keywords:
Microturbine
Steam injection
Thermal power modulation
Gasturbines
Combined heat and Power

ABSTRACT

This paper reports on a series of steam injection experiments on a Turbec T100 microturbine. Combined Heat and Power (CHP) systems, such as the considered T100 microturbine, use one single primary fuel to simultaneously produce electric and thermal power. In doing so, they realize significant energy savings compared to conventional schemes of separated production. However, a reduction in the demand for heat (e.g. in summertime) will force this type of units to shutdown. This significantly reduces the amount of operating hours and has a severe negative impact on the net present value of such CHP investment projects.

The aim of this paper is to investigate and demonstrate the effects of steam injection in the compressor outlet of a microturbine operating under reduced heat demand conditions, in order to keep the unit running. The necessary steam can be auto-raised with heat available in the turbine exhaust downstream of the recuperator. Such an injection will keep the unit running and thus avoid a forced shutdown. Furthermore, it is expected that the electric efficiency will rise and that the power production will become more economically viable as a result of the increasing operating hours.

This paper reports on the influence of steam injection on the electrical efficiency and shaft speed of a T100 unit. ASPEN® simulations of the behavior of the CHP unit are also presented. These simulations predicted a 2.2% rise in electric efficiency at nominal electrical output when 5% of the mass flow rate of air is replaced by steam.

The steam injection experiments resulted in stable runs of the unit, a predicted reduction in shaft speed and increasing electrical efficiency. Validation of the ASPEN® simulations against the experimental data revealed the necessity for a more accurate determination of the air mass flow rate and more precise compressor characteristics.

1. Introduction

Microturbines are in general cost effective [1,2], but in our specific (residential) case, the attractiveness of the investment depends strongly on the yearly amount of running hours of the unit. A non-continuous heat demand reduces the amount of yearly running hours and negatively affects the profitability. Current research on improving microturbine efficiency focuses mainly on improving the thermal resistance of the inner microturbine parts and on recuperator designs with increased heat exchanger efficiency [3–5]. This paper presents an alternative route to increase the yearly amount of running hours. By injection of steam, auto-raised with the available heat in the turbine exhaust, the fuel consumption can be reduced during hotter periods with reduced heat demand. The injection of steam increases electric efficiency of the unit and more importantly avoids the shutdown of the unit. This increases the engine running hours, which has a positive impact on the net present value, resulting in a more interesting Combined Heat and Power (CHP) investment project [6].

2. Approach

In previous work [6], the dry and wet operation of the T100 microturbine were simulated with the ASPEN® plus process simulation tool (Version 2006.5). Dry simulations were compared with experiments for validation. In this work, experiments on the T100 microturbine were performed to validate the wet simulations. Wet simulations predicted a 2.2% rise in electric efficiency at nominal electrical output if 5% of the mass flow rate of air is replaced by steam.

In a first step, an analytic perturbation model was set up to accurately calculate changes in microturbine parameters and overall efficiency. Based on the variation of the shaft speed and the injected steam flow, the perturbation of all parameters can be calculated accurately. Verification of the model was performed by comparing it to the ASPEN® simulations [6].

* Corresponding author. Tel.: +32 2 6293182; fax: +32 2 6292865.
E-mail address: wdepaepe@vub.ac.be (W. De Paepe).

0306-2619/$ - see front matter © 2012 Elsevier Ltd. All rights reserved.
doi:10.1016/j.apenergy.2012.01.051

Nomenclature

CAF	corrected air flow, defined as $\dot{m}_{air}\sqrt{T_1}/p_1$ (kg$\sqrt{K}$/s/bar)
CHP	Combined Heat and Power
C_p	heat capacity (J/kg K)
HRSG	Heat Recovery Steam Generator
LHV	lower heating value (MJ/kg)
k	specific heat ratio, C_p/C_v
$\dot{m}_{air}$	air mass flow (kg/s)
$\dot{m}_{comp}$	mass flow through compressor (kg/s)
$\dot{m}_{fluegas}$	flue gas mass flow (kg/s)
$\dot{m}_{fuel}$	fuel mass flow (kg/s)
$\dot{m}_{steam}$	injected steam mass flow (kg/s)
$\dot{m}_{turb}$	mass flow through turbine (kg/s)
N	compressor shaft speed (%) of nominal speed
p	pressure (bar)
PIT	turbine inlet pressure (bar)
POT	turbine outlet pressure (bar)
T	temperature (°C)
TIT	turbine inlet temperature (°C)
TOT	turbine outlet temperature (°C)
$\dot{W}_{comp}$	power consumed by compressor (kW)
$\dot{W}_{el}$	delivered net electrical power (kW)
$\dot{W}_{turb}$	delivered turbine power (kW)

Greek symbols

π	pressure ratio, defined as p_2/p_1

Subscripts

1	conditions at compressor inlet
2	conditions at compressor output
4	conditions at recuperator outlet
comp	conditions inside compressor
fluegas	conditions of flue gases
is	isentropic conditions
ref	dry reference case
steam	condition of injected steam
turb	conditions inside turbine
Surge	conditions at surge limit
Working	conditions at operating point

In a second step, experiments with externally produced steam were performed on the T100 microturbine at nominal and partial load. Measurements were used to validate the ASPEN® model simulations.

3. Microturbine layout

Fig. 1 shows the standard microturbine layout. After entering the compressor (1), the compressed air enters the recuperator (2) for partially recuperating residual heat from the flue gases. Fuel is injected in the combusting chamber in order to raise temperature till the maximum turbine inlet temperature (3). Behind the air recuperator, a secondary heat exchanger provides hot water for residential heating purposes (4). Through a single shaft, the microturbine is connected to a high-speed electric generator. The power output of the generator is adapted by power electronics to deliver 50 Hz electricity.

4. Experimental setup

The experiments were performed using a Turbec T100 microturbine, with a nominal power output of 100 kW. The microturbine produces a fixed electrical power output by adjusting its rotation speed. Table 1 reports the thermodynamic conditions of the T100 at each stage of its cycle in Fig. 1, in nominal 'dry' mode and in nominal 'wet' mode.

Microturbine electric efficiency is calculated using Formula (1)

$$\eta_{el} = \frac{\dot{W}_{el}}{\dot{m}_{fuel} LHV} \tag{1}$$

Although externally produced steam is injected in the microturbine during the described tests in this paper, the energy from the injected steam is not considered in efficiency calculations (see Eq. (1)). In the final lay-out of the microturbine, the goal is to use steam, auto-raised in a low pressure steam generator with the available heat in the turbine exhaust (see Fig. 1). The amount of injected steam, externally produced with a steam generator, as described in paragraph 4.2, matches the maximum possible amount of steam that can be auto-raised, using a Heat Recovery Steam Generator (HRSG). For the lab setup however, no HRSG was installed for steam production. Instead, an electric steam generator was used to produce the necessary steam in order to obtain a higher flexibility in the injected steam mass flow during the test. The steam generator also allows a better insight in the experiments.

A Diris multimeter (Socomec) is used to measure the generated electric power with an accuracy of 1%. The LHV of the fuel was provided by the fuel supplier on a daily basis, together with the composition. Based upon this composition, the LHV has been recalculated in ASPEN®, resulting in a difference of 0.17% with the LHV provided by the supplier. An Actaris diaphragm meter (accuracy 0.5%) measures the fuel flow, resulting in an absolute error on the electric efficiency of 0.5%. The injected amount of steam is very small (maximum 5% of the total mass flow of air) and the predicted rise in efficiency is 0.44% per injected steam fraction[1] at nominal load, resulting in a very small change in fuel flow (2% less fuel consumption). The fuel flow meter is however incapable of accurately measuring this small variation in fuel flow. This problem can be solved using an analytical perturbation analysis.

In this perturbation model, an analytical model of the microturbine is built, in order to accurately calculate the efficiency rise. Starting from a *reference case* (dry case, ψ_{ref}), which is perturbed by steam injection, the new condition (called the *adapted case*, $\psi_{adapted}$) is calculated using only perturbation ($\delta\psi$) of accurate measurable parameters. (Rotation speed N and injected steam flow $\dot{m}_{steam}$) (see Formula (2))

$$\psi_{adapted} = \psi_{ref} + \delta\psi \tag{2}$$

4.1. Perturbation analysis

The electric efficiency of the microturbine can be calculated using Formula (1). When water is injected in the microturbine, electric power will rise, but the T100 delivers constant output power, so the controller will interfere and adjust the injected fuel in the combustion chamber. Thus, the rise in efficiency caused by steam injection can be calculated using Eq. (3) (produced electric power remains constant).

$$\frac{\delta\eta_{el}}{\eta_{el,ref}} = -\frac{\delta\dot{m}_{fuel}}{\dot{m}_{fuel,ref}} \tag{3}$$

[1] Steam fraction is equal to $\frac{\dot{m}_{steam}}{\dot{m}_{total}}$ with $\dot{m}_{total} = \dot{m}_{comp} + \dot{m}_{steam}$, taking into account the decreasing airflow because of the decreasing shaft speed.

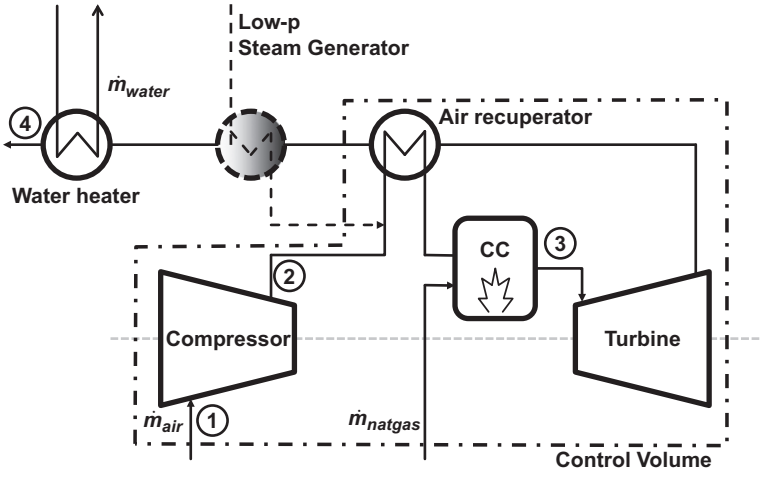

Fig. 1. Microturbine layout.

Table 1
Thermodynamic conditions of the T100 at each stage of the cycle.

	Dry mode[a,b]	Wet mode[a,c]
Compressor		
T_{in}	15 °C	15 °C
p_{in}	1.013 bar	1.013 bar
T_{out}	195.8 °C	188.9 °C
p_{out}	4.199 bar	4.012 bar
$\dot{m}_{comp}$	0.706 kg/s	0.656 kg/s
$\dot{W}_{comp}$	130.1 kW	116.3 kW
Recuperator		
$T_{in,cold}$	195.8 °C	186.1 °C
$T_{in,hot}$	645 °C	645 °C
$T_{out,cold}$	574.5 °C	573.6 °C
$T_{out,hot}$	283.2 °C	274.5 °C
$\dot{Q}_{rec}$	286.9 kW	290.3 kW
Combustion chamber		
T_{out}	917.4 °C	903.6 °C
p_{out}	3.779 bar	3.610 bar
$\dot{m}_{fuel}$	6.15 g/s	5.90 g/s
Turbine		
T_{out}	645 °C	645 °C
p_{out}	1.05 bar	1.05 bar
$\dot{m}_{turb}$	0.712 kg/s	0.684 kg/s
$\dot{W}_{turb}$	230.1 kW	216.3 kW
Steam		
$\dot{m}_{steam}$	/	0.022 kg/s
T_{steam}	/	145.8 °C
p_{steam}	/	4.012 bar
Steam status	/	Saturated
Global		
$\dot{W}_{el}$	100.0 kW	100.0 kW
η_{el}	32.60%	33.92%
N	67,245 rpm	65,794 rpm
$\dot{Q}_{thermal}$	170.1 kW	98.3 kW
$\eta_{thermal}$	55.3%	33.3%
T_{stack}	55 °C	55 °C

[a] Results calculated using the ASPEN® process simulator.
[b] 'Dry mode' corresponds to the normal CHP mode of the microgasturbine, running at nominal electric power.
[c] 'Wet mode' corresponds to the steam injected case. The thermodynamic conditions given in the table correspond to the maximal adiabatic steam injection possible (steam fraction of 3.3%).

$\delta\dot{m}_{fuel}$ has to be calculated, for the aforementioned reasons. The goal of the perturbation analysis is to find an expression: $\delta\dot{m}_{fuel} = f(\delta N, \delta\dot{m}_{steam})$, where $\delta\dot{m}_{fuel}$ is only a function of accurately measurable perturbations $(\delta N, \delta\dot{m}_{steam})$. This means that all parameters of the microturbine have to be expressed as a function of the changes in rotational speed and injected steam flow.

In a first step, all perturbations of parameters from the turbine and compressor are expressed as a function of δN and $\delta\dot{m}_{steam}$. The problem, however, is that all parameters are linked, so a system of equations has to be created and solved.

A first set of equations is given by the controller of the microturbine. During operation, the controller keeps the electric output constant. In order to keep the electrical efficiency as high as possible, *TIT* should be maximal. To do this, *TOT* is controlled and kept constant.

$$\|\dot{W}_{turb}\| - \|\dot{W}_{comp}\| = \|\dot{W}_{el}\| \ (constant) \tag{4}$$

$$TOT = constant \tag{5}$$

The turbine inlet is assumed to be choked, resulting in Eq. (6).

$$\frac{\dot{m}_{turb}\sqrt{TIT}}{PIT} = A\sqrt{\frac{k_{turb}}{R}}\left(\frac{2}{k_{turb}+1}\right)^{\frac{k_{turb}+1}{2(k_{turb}-1)}} = constant \tag{6}$$

During steam injection experiments, the composition of the exhaust gas will change significantly, resulting in a changing specific heat ratio, k_{turb} and thus a change in the chocking constant. Calculations of this changing condition at maximal steam injection rate showed however a maximal variation of less than 0.01% of the absolute change in efficiency. For further calculations, the value of the chocking constant in Eq. (6) was kept constant, which seems an acceptable assumption.

Energy conservation expressed over compressor and turbine gives following equations:

$$\|\dot{W}_{turb}\| = \dot{m}_{turb}C_{p,turb}(TIT - TOT) \tag{7}$$

$$\|\dot{W}_{comp}\| = \dot{m}_{comp}C_{p,comp}(T_2 - T_1) \tag{8}$$

Isentropic laws express the relation between in- and outlet of compressor and turbine resulting in another four equations.

$$\frac{TOT_{is}}{TIT} = \left(\frac{POT}{PIT}\right)^{\frac{k_{turb}-1}{k_{turb}}} \tag{9}$$

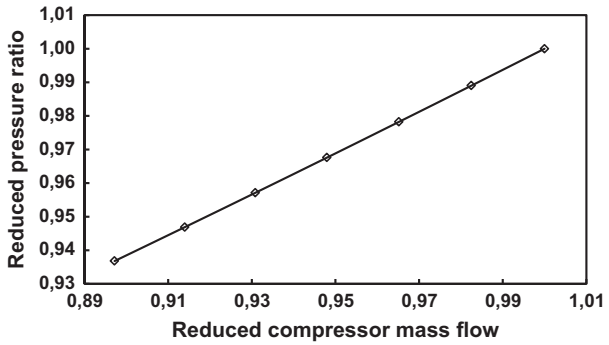

Fig. 2. Change of the operating point of the compressor through steam injection. This curve has been drawn at variable rotation speed N and constant TOT and chocking condition.

$$\frac{T_{2,is}}{T_1} = \left(\frac{p_2}{p_1}\right)^{\frac{k_{comp}-1}{k_{comp}}} \tag{10}$$

$$\eta_{is,turb} = \frac{TIT - TOT}{TIT - TOT_{is}} \tag{11}$$

$$\eta_{is,comp} = \frac{T_{2,is} - T_1}{T_2 - T_1} \tag{12}$$

Compressor and turbine efficiency ($\eta_{is,turb}$, $\eta_{is,comp}$) are assumed to be constant. ASPEN® simulations of the steam injection showed that with a steam injection ratio of 5%, the pressure ratio and mass flow of the compressor change less than 10% (Fig. 2). On the generic compressor map (Fig. 3), the efficiency of the compressor does not change in the zone around the dry operating point.

The link between the compressor and the turbine is given by the pressure. A small pressure drop in the combustion chamber, between compressor and turbine is assumed. POT is constant and slightly above atmospheric pressure.

$$PIT = 0.9p_2 \tag{13}$$

$$POT = constant \tag{14}$$

Eqs. (4)–(12) can be found in [7].

Differentiating Eqs. (4)–(14) results in a set of 11 equations with 12 unknown perturbations δ. To solve this set of equations, a 12th equation is necessary. This 12th equation is given by the generic compressor map. This equation expresses the link between shaft speed, air flow and pressure ratio of the compressor. The compressor map is made analytical by fitting super ellipses with the generic map [8].

$$\left(\frac{CAF}{a}\right)^z + \left(\frac{\pi - 1}{b - 1}\right)^z = 1 \tag{15}$$

where a equals the corrected air flow when pressure ratio equals 1, just like b is equal to the pressure ratio when the mass flow decreases to zero. Both conditions could never be reached, because of the surge and chocking limits of the compressor. Differentiating Eq. (15) results in the necessary 12th equation. The system of equations can be solved and the perturbation of all turbine and compressor parameters can now be expressed as a function of δN and $\delta\dot{m}_{steam}$.

In a second step, by expressing and differentiating the energy balance over a control volume (Fig. 1), an expression for the change in fuel consumption as function of known perturbations, calculated in the previous step, is obtained (Eq. (18)).

The energy balance over the control volume indicated in Fig. 1:

$$\begin{aligned}&\dot{m}_{comp}C_{p,air}(T_1 - T_{ref}) + \dot{m}_{fuel}LHV \\ &\quad = \dot{W}_{el} + \dot{Q}_{loss} + (\dot{m}_{turb} - \dot{m}_{steam})C_{p,fluegas}(T_4 - T_{ref}) \\ &\qquad + \dot{m}_{steam}C_{p,steam}(T_4 - T_{inj})\end{aligned} \tag{16}$$

And after differentiating, the energy balance becomes:

$$\begin{aligned}&\delta\dot{m}_{comp}C_{p,air}(T_1 - T_{ref}) + \delta\dot{m}_{fuel}LHV \\ &\quad = (\delta\dot{m}_{turb} - \delta\dot{m}_{steam})C_{p,fluegas}(T_4 - T_{ref}) + \delta\dot{m}_{steam}C_{p,steam}(T_4 \\ &\qquad - T_{inj}) + (\dot{m}_{turb} - \dot{m}_{steam})C_{p,fluegas}\delta T_4 + \dot{m}_{steam}C_{p,steam}\delta T_4\end{aligned} \tag{17}$$

Rearranging Eq. (17) results in an expression for $\delta\dot{m}_{fuel}$.

$$\begin{aligned}\delta\dot{m}_{fuel} = \big[&(\delta\dot{m}_{turb} - \delta\dot{m}_{steam})C_{p,fluegas}(T_4 - T_{ref}) + \delta\dot{m}_{steam}C_{p,steam}(T_4 - T_{inj}) \\ &+ (\dot{m}_{turb} - \dot{m}_{steam})C_{p,fluegas}\delta T_4 + \dot{m}_{steam}C_{p,steam}\delta T_4 \\ &- \delta\dot{m}_{comp}C_{p,air}(T_1 - T_{ref})\big]/LHV\end{aligned} \tag{18}$$

The only remaining problem is the unknown temperature in between the recuperator and the water heater (T_4). Using the LMTD-method [9], the specification of the recuperator given in [10] and

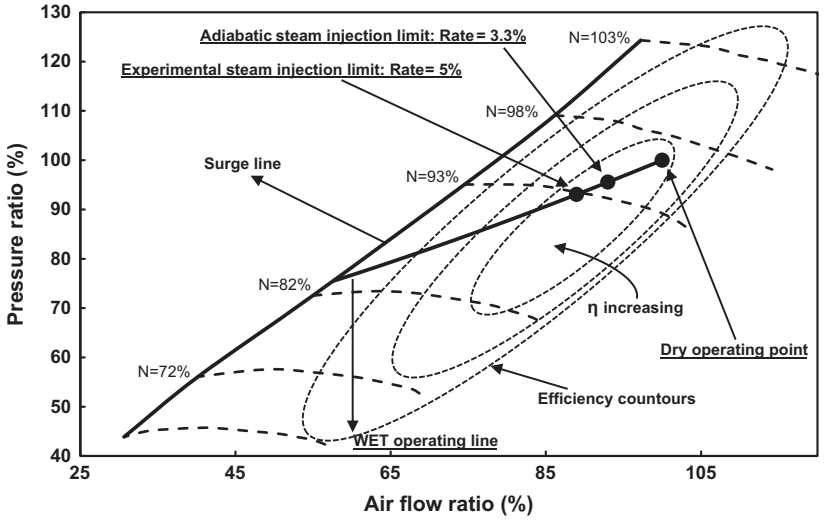

Fig. 3. Generic compressor map. The 'Dry operating point' corresponds to the operation of the gasturbine at nominal power (100 kW) and 15 °C inlet temperature and 1.013 bar inlet pressure.

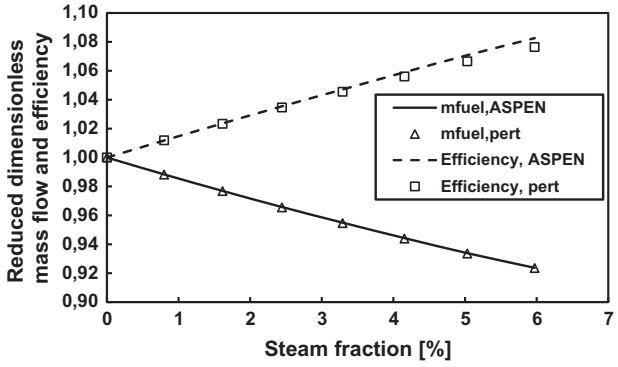

Fig. 4. Perturbation analysis compared with ASPEN® simulation results.

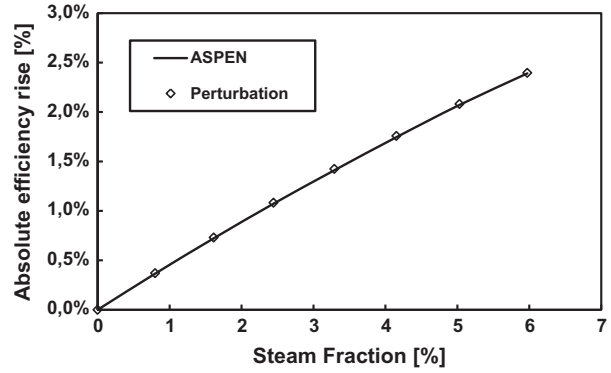

Fig. 5. Predicted increasing efficiency by perturbation analysis compared with ASPEN® simulated absolute efficiency rise.

the hypotheses from [11], the temperature of the flue gases at the recuperator outlet could be calculated. Once δT_4 is known, the change in fuel consumption can be calculated.

The results of the analytical perturbation analysis were compared with the results of the ASPEN® simulations for validation as shown in Figs. 4 and 5.

The aim of the perturbation analysis is to reduce the error on the change in measured fuel consumption in order to have an accurate estimation of the rise in efficiency. To estimate the error on $\delta\dot{m}_{fuel}$ in the perturbation analysis, a 'what if'-analysis was performed. For this 'what if'-analysis, it was necessary to know the relative errors on the measured shaft speed and the mass flow of injected steam. By letting the input values of the perturbation model $(\delta N, \delta\dot{m}_{steam})$ vary between their limits of uncertainty, the maximal and minimal possible efficiency rise can be calculated. Out of these maxima, the uncertainty on the final result can be predicted. The shaft speed of the compressor is measured through an optical technique with an accuracy of 0.01% of the nominal shaft speed. The incoming steam flow is measured with a Yokogawa flow vortex meter with an accuracy of 1%. The 'what if'-analysis results in Table 2 show that the difference between the rise in efficiency – calculated with the exact 'measured' values from the ASPEN® simulations – and the maximal rise in efficiency – calculated using values between the uncertainty limits of the input perturbations – is very small. This gives rise to an accuracy of 0.9% on the absolute rise in efficiency for the perturbation analysis. This will make it possible to calculate the change in efficiency in a very accurate way.

4.2. Steam generator

To produce the necessary steam, an Osbyparca electric steam boiler is used. The maximum electrical power of the steam boiler was chosen in function of the maximal heat that could be recovered from the hot flue gases in the HRSG. This power was calculated via a pinch analysis [12], using a pinch of 25 °C and taking into account that through steam injection, the total air flow through the engine will decrease and that the temperature of the flue gases after the recuperator will as well because of the additional water in the incoming cold flow. Pinch analysis calculations showed that the adiabatic steam injection limit corresponds to an injection rate of 3.3%. The main specifications of the electrical steam boiler are given in Table 3. The steam boiler produces saturated steam with a pressure corresponding to the set point.

The saturated steam (around 140 °C) from the steam generator is injected in the microturbine behind the compressor, but before the recuperator in the compressed air at around 180 °C. The steam boiler does not actively control the injected steam flow; the steam flow is determined by the pressure difference between the steam boiler and the compressor outlet. Once the pressure in the boiler surpasses the compressor outlet pressure, steam is injected. However, if the pressure after the compressor alters, the injected mass flow rate of steam will immediately adapt itself to the new conditions. A possible solution to avoid this unwanted fluctuation is a higher pressure in the steam boiler, resulting in a choked and constant steam flow. To achieve this choking condition, the pressure in the steam boiler needs to be much higher.

The water level inside the boiler is kept constant with an auxiliary pump with adaptable shaft speed and flow rate. Based upon the outgoing steam flow rate, the frequency of the pump can be set. When a constant hot steam flow is leaving the boiler, the pump will inject the same amount of cold water. This leads to a steady operating condition inside the boiler. In turn, this will keep the temperature and pressure constant, resulting in a constant outgoing steam flow. The outgoing steam flow is measured, as mentioned in the previous paragraph, with a Yokogawa flow vortex meter with an accuracy of 1%. The measurements of the outgoing steam flow of the electric boiler have been checked, using the ingoing electric energy of the boiler. By comparing these measurements with the outgoing energy of the steam flow, calculated based upon the measured steam flow, the measured steam temperature and the fact that the steam is saturated, only a small difference between both was noticed.

Table 2
Results of the 'What-if' analysis.

Steam flow (g/s)	ASPEN[a] (%)	Perturbation[b] (%)	What-if analysis[c] (%)	Absolute error[d] (%)	Relative accuracy[d] (%)
35[e]	2.39	2.39	2.41	0.02	0.9

[a] Simulated rise in efficiency in ASPEN®.
[b] Calculated rise in efficiency with the perturbation analysis model, using the exact perturbation from the ASPEN® simulations.
[c] Calculated rise in efficiency with the perturbation analysis model, by letting the exact perturbation from the ASPEN® simulations vary between their limits of uncertainty.
[d] Compared to the ASPEN® results.
[e] Maximal steam flow injected during reported experiments.

Table 3
Specifications of the electric steam boiler.

Voltage	3 * 400 V
Nominal power	96 kW
Number of power stages	4
Operating pressure	7 bar

5. Test procedure and conditions

Before experiments with steam injection could be started, one should mention two major limitations on steam injection: compressor surge and combustion instabilities.

In industrial gas turbines, steam injection in a gas turbine will lead to an increase of the compressor discharge pressure [13]. This increase causes a surge margin reduction [14]. Surge margin is defined via Eq. (19), according to Walsh and Fletcher [15].

$$SM(\%) = \frac{\pi_{comp,surge} - \pi_{comp,working}}{\pi_{comp,working}} \cdot 100\% \quad (19)$$

The operating line by injecting steam at full load is added in Fig. 3. The operating line is extended beyond the adiabatic limit of 3.3% steam injection by means of adding steam raised through an external heat source to examine the maximum potential steam injection in this engine. As mentioned by Delattin et al. [6], no surge problems are expected when auto-raised steam is injected in the T100 microgasturbine. From Fig. 3, it can be computed that the surge margin drops from 30% to 22% when the CHP mode is completely disabled and the adiabatic steam injection limit is reached. For the experiments discussed in this paper, steam injection was extended beyond this limit. At maximal injected steam flow (0.035 kg/s steam, 5% steam fraction), the surge margin will drop further till 20%, which demonstrate the ability of the microturbine to run safely in wet operation.

Since steam is introduced in the microgasturbine, a second possible issue is the stability of the combustion. The possible combustion instability and the reduced combustion efficiency may cause increasing emissions of carbon monoxide and unburned hydrocarbons [16]. A summary of the performed research on this topic is given by Jonsson and Yan [16]. The authors report that research showed low emission levels of carbon monoxide, except at high humidification levels [17]. All researchers [17–21], mentioned by Jonssen and Yan [16], showed a reduction of NO_x emissions, due to a lower equilibrium temperature and the increasing concentrations of OH atoms [18]. For this paper, the moisture level in the air was limited (5%), so no problems were expected with combustion stability and emission levels.

The experimental validation of the simulations of the steam injection consists of two major experiments. A first experiment was done at partial electrical load. Because of the unadjusted controller of the T100, some precautions must be taken. After successful injection of steam at partial load (80 kWe), a second experiment was set up, to inject steam at nominal electrical power. Test procedure for both experiments was initially the same and as follows: The T100 was started and ran for over half an hour dry, in order to have a dry reference so the electric efficiency rise could be calculated exactly, because efficiency of the microturbine is function of the inlet air temperature. After this 'run in' period, steam was injected. The maximum pressure inside the boiler was raised above the pressure after the compressor. Electrical power of the boiler was set to the minimum, in order to minimize the first injection flow. After a period, the power input of the boiler was raised and steam injection flow increased. Fig. 6 shows the result of the steam injection.

Initiating the injection of steam in the engine at nominal power was not possible, as predicted by the simulations. The simulations of the dynamic behavior of the microturbine showed that the sudden injection of steam at full load provoked an automatic shutdown by the unadapted control system of the unit. When steam is injected in the microturbine, more power will be available at the shaft. This extra power allows the microturbine to speed up and generate more electrical power. At this point, the controller will interfere and slow down the engine by decreasing the fuel flow. At nominal speed however, the safety margin of the controller is narrower. When steam is injected at nominal speed, the sudden increasing rotation speed and produced electrical power is seen by the controller as a microturbine going in overspeed and the controller will consequently shut down the engine. Unfortunately, the shaft speed is recorded by the engine monitoring system only every 90s, making it impossible to notice this phenomenon. For the second experiment, another steam injection protocol was utilized. From the first experiment, it appeared that the control system of the engine was able to handle the initiation of steam injection at 80 kW part load. Therefore, it was decided to start the steam injection at 80 kW part load condition followed by a slow and steady increasing electric power demand towards 100 kW. While doing so, steam was injected successfully in this second experiment. After the steam injection was stopped, the engine was kept running for some time in dry mode, this in order to obtain post-run data for dry engine operation at nominal load.

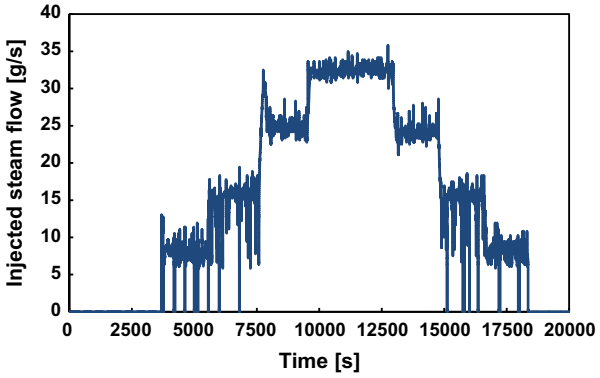

Fig. 6. Measured steam flow.

6. Test results

As predicted by the simulations, the shaft speed reduces by injecting steam. Fig. 7 shows the decreasing shaft speed as function of the steam injection rate for experiment 1 (experiment performed at 80 kW part load).

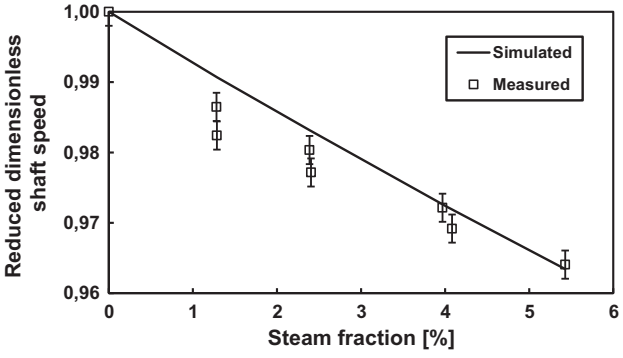

Fig. 7. Shaft speed during steam injection.

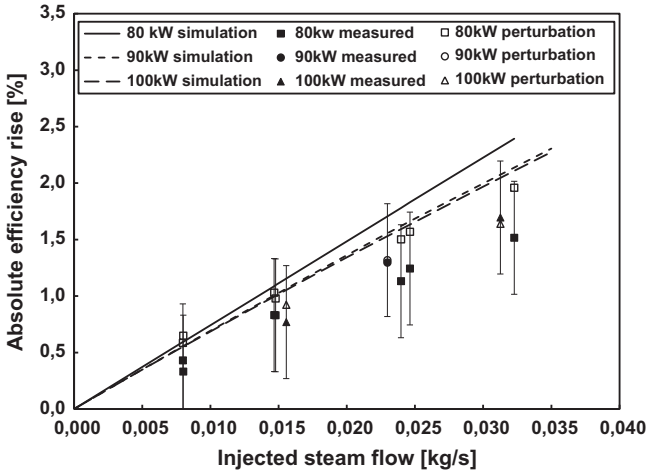

Fig. 8. Measured and calculated part load and nominal load efficiency.

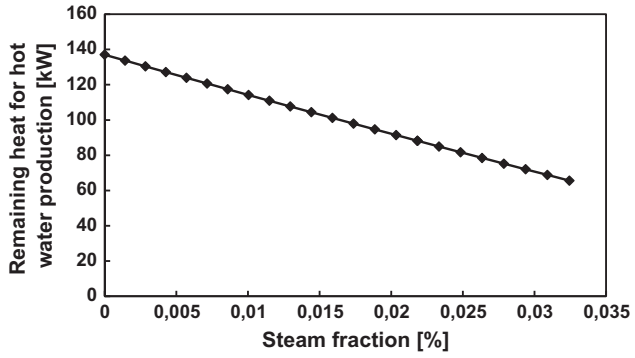

Fig. 9. Simulated remaining heat for hot water production during steam injection, using a final stack temperature of 55 °C.

Using Eq. (1), the electrical efficiency could be calculated for both experiments. Fig. 8 shows the results compared with the ASPEN® simulations.

As it can be seen on Fig. 8, the errors on the directly calculated efficiency values are very large. Therefore, it is of no use to compare simulated values with calculated values because the variance on the calculated efficiency rise is of the same order of magnitude as the rise itself. This illustrates very well the need for the perturbation analysis approach presented in this paper because – as can be seen on the same figure – the errors on the values obtained via the perturbation analysis are much smaller (0.02% absolute error on absolute electric efficiency rise).

As the steam injection ratio would increase, the remaining heat for hot water production will decrease, because most of the heat will be used for steam production in the HRSG. Fig. 9 gives the available heat for hot water production depending on the steam injection ratio, simulated in ASPEN®. Results given in Fig. 9 are simulated, using a final exhaust gas temperature of 55 °C, which is the standard stack temperature for water heating with incoming water at 50 °C and leaving hot water at 70 °C. At maximal adiabatic steam injection flow rate (3.3%), the remaining heat for hot water production is 98 kW. Validation of these simulations by measurement however was not the scope of this paper.

7. Conclusions

As it can be concluded from Fig. 8, the simulation model of the steam injection in the microturbine is too optimistic about the efficiency rise through steam injection. In reality, not the predicted 0.44 ± 0.02% efficiency rise per 1% steam fraction injected at nominal power, but a lower 0.34 ± 0.02% was observed. Efficiency therefore increases less than expected. Two explanations are possible for the lower efficiency gain:

The first explanation is that the real mass flow rate through the compressor is not measured. Therefore, for the calculations in the perturbation analysis, the values obtained from the ASPEN® simulation were used. It is possible that ASPEN® underestimates this compressor mass flow rate.

A second explanation is the use of generic compressor and turbine maps for the ASPEN® model. The ingoing air and fuel mass flow rate and the generated power are all derived from the characteristics on these maps. There is a degree of uncertainty to which extent the utilized generic maps are in accordance with the real characteristics of this engine.

8. Discussion and future work

The steam injection experiments resulted in stable runs of the engine, a predicted reduction in shaft speed and increasing electrical efficiency. However, the validation of the ASPEN® simulations against the experimental data revealed that the simulations were too optimistic. Efficiency increased less than expected with steam injection. This validation revealed the necessity for a more accurate determination of the air and fuel mass flow rate and more precise compressor maps. The next step will be the more precise measurements of these parameters.

Acknowledgement

The research was funded by the FWO (Fonds voor Wetenschappelijk Onderzoek).

References

[1] Gamou S, Yokoyama R, Ito K. Parametric study on economic feasibility of microturbine cogeneration systems by an optimization approach. J Eng Gas Turbines Power 2005;127:389–96.
[2] Katsigiannis PA, Papadopoulos DP. A general technoeconomic and environmental procedure for assessment of small-scale cogeneration scheme installations: application to a local industry operating in Thrace, Greece, using microturbines. Energy Convers Manage 2005;46:3150–74.
[3] Massardo AF, McDonald CF, Korakianitis T. Microturbine/fuel-cell coupling for high-efficiency electrical-power generation. J Eng Gas Turbines Power 2002;124:110–6.
[4] McDonald CF. Low-cost compact primary surface recuperator concept for microturbines. Appl Therm Eng 2000;20:471–97.
[5] McDonald CF. Recuperator considerations for future higher efficiency microturbines. Appl Therm Eng 2003;23:1463–87.
[6] Delattin F, Bram S, Knoops S, De Ruyck J. Effects of steam injection on microturbine efficiency and performance. Energy 2008;33:241–7.
[7] Çengel YA, Boles MA. Thermodynamics: an engineering approach. McGraw-Hill; 2006.
[8] Haugwitz S. Modelling of microturbine systems. Lund Institute of Technology, PhD thesis; May 2002.
[9] Çengel YA. Heat and mass transfer: a practical approach. McGraw-Hill; 2006.
[10] Lagerstrom G, Xie M. High performance and cost effective recuperator for micro-gas turbines. In: ASME conference proceedings; 2002. p. 1003–7.
[11] Hahn A. Modeling and control of solid oxide fuel cell – gas turbine power plant systems. University of Pittsburgh. Master thesis; April 2000.
[12] Linnhoff B. Engineers IoC. A user guide on process integration for the efficient use of energy. Institution of Chemical Engineers; 1994.
[13] Mathioudakis K. Analysis of the effects of water injection on the performance of a gas turbine. J Eng Gas Turbines Power 2002;124:489–95.
[14] Roumeliotis I, Mathioudakis K. Evaluation of water injection effect on compressor and engine performance and operability. Appl Energy 2010;87:1207–16.
[15] Walsh PP, Fletcher P. Gas turbine performance. Blackwell Science; 2004.
[16] Jonsson M, Yan J. Humidified gas turbines—a review of proposed and implemented cycles. Energy 2005;30:1013–78.
[17] Hermann F, Klingmann J, Gabrielsson R. Computational and experimental investigation of emissions in a highly humidified premixed flame. In: ASME conference proceedings; 2003. p. 819–27.

[18] Bhargava A, Colket M, Sowa W, Casleton K, Maloney D. An experimental and modeling study of humid air premixed flames. J Eng Gas Turbines Power 2000;122:405–11.
[19] Day W, Kendrick D, Knight B, Bhargava A, Sowa W, Colket M, et al. HAT cycle technology development program. Advanced turbine systems annual program review meeting; 1999.
[20] Chen AG, Maloney DJ, Day WH. Humid air NO_x reduction effect on liquid fuel combustion. J Eng Gas Turbines Power 2004;126:69–74.
[21] Traverso A, Massardo AF. Thermoeconomic analysis of mixed gas–steam cycles. Appl Therm Eng 2002;22:1–21.